Supporting Information

In situ evaluation of calcium phosphate nucleation kinetics and pathways during intra and extrafibrillar mineralization of collagen matrices

Doyoon Kim,[†] Byeongdu Lee,[‡] Stavros Thomopoulos,[§] and Young-Shin Jun*[,†]

[†] Department of Energy, Environmental & Chemical Engineering, Washington University, St. Louis, Missouri 63130, United States

[‡] X-ray Science Division, Argonne National Laboratory, Argonne, Illinois 60439, United States

[§] Department of Orthopedic Surgery, Columbia University, New York, New York 10032-3072, United States

*****E-mail: ysjun@seas.wustl.edu*

Table of Contents:

Experimental Section ····· **S2**

Table S1. Ionic components of simulated body fluids and human blood plasma····· **S3**

Figure S1. Experimental setup for collagen mineralization and SAXS/WAXS measurements ····· **S6**

Figure S2. Background SAXS intensities ····· **S12**

Figure S3. SAXS intensities from mineralized collagen matrices and their fittings····· **S13**

Figure S4. WAXS intensities from mineralized collagen matrices at z = 0–0.3 mm and synthetic hydroxyapatite ····· **S15**

Figure S5. TEM images of stained thin sections of MC0p and MC10p at a late stage of mineralization ····· **S16**

***Ex situ* analyses of CaP distribution within the collagen matrices at a late stage of the mineralization** ····· **S18**

Figure S6. SEM images and corresponding Raman spectra of collagen matrices····· **S20**

Table S2. Atomic ratios of mineralized collagen at different positions on cross sections, from SEM-EDS ····· **S22**

References ····· **S23**

Experimental Section

Preparation of samples. Collagen matrices were reconstituted based on a previously published method.[1] Type I collagen (C857, calf skin lyophilized, Elastin Products Company, Inc.) was dissolved in 0.5 mM HCl (12 mg ml^{-1}) by magnetic stirring, followed by degassing under vacuum for 4 days. Collagen samples were maintained at 4ºC during this process. Then the collagen solution was placed in a specially designed polytetrafluoroethylene frame with a #1 cover glass on one side, and the frame was placed for an hour in TES buffered saline (5.5, 6.32, and 3.4 g l^{-1} of TES, NaCl, and Na_2HPO_4, in deionized water, pH 7.5 at 37ºC). The frame was then stored in deionized water overnight to remove excess salt, and the opposite side was capped with another glass. The cover glass held the solution and collagen, and also allowed X-ray penetration during the X-ray scattering analysis. The frame was 2 mm thick in the direction of the X-ray path. The collagen matrices were 10 mm wide and 5 mm high. The cover glasses were 3 mm taller than the matrices, to contain sufficient simulated body fluids (SBF) to prevent collagen dehydration during the X-ray scattering analysis (Figure 1a). To reconstitute the lyophilized collagen in a well-controlled shape with uniform thickness for the SAXS evaluations, a collagen fibrillar density of 12 mg ml^{-1} was used. With this collagen fibrillar density, we were able to observe both intra and extrafibrillar mineralization behaviors clearly in the mineralization solution.

In addition, thin collagen films (only applied for Figure 6) were prepared on glass slides to simulate the reaction occurring at the outermost surface of collagen matrices, which were not analyzed from sections cut along the *z*-direction. To prepare a film, a droplet (0.1 ml) of dissolved collagen (12 mg ml^{-1} of collagen in 0.5 mM HCl) was evenly dispersed on a glass slide (1×1 cm^2) using a spin coater (Laurell WS-650MZ-23NPP, 5000 rpm for 30 s). Then the slide was placed in the TES buffered saline for an hour to polymerize collagen fibrils. The prepared film on glass was

stored in deionized water, as was done for collagen matrices. CaP structures formed during the collagen mineralization were compared with synthetic hydroxyapatite sample (ACROS Organics™).

Simulated body fluid and the flow-through reactor. A simulated body fluid proposed by Kokubo *et al*. (1×SBF) is commonly used because of its similarity in ionic components to human body plasma.[2,3] To conduct our experiments within a reasonable time, we used an SBF with three times higher concentrations of calcium and phosphate ions (3×SBF) as an experimental solution. The ionic compositions of 1×SBF, 3×SBF, and human blood plasma are listed in Table S1. American Chemical Society grades of NaCl (7.996 g, BDH Chemicals), $NaHCO_3$ (0.350 g, BDH Chemicals), KCl (0.224 g, BDH Chemicals), $MgCl_2 \cdot 6H_2O$ (0.305 g, EMD Millipore), 1 M HCl (40 ml, BDH Chemicals), Na_2SO_4 (0.071 g, Alfa Aesar), tris(hydroxymethyl)aminomethane (Tris, 6.057 g, Alfa Aesar) were added to 900 ml of deionized water (18.2 M Ω cm^{-1}). Either 0 or 10 mg of polyaspartic acid, pAsp (sodium salt, M_w: 5,000 Da, LANXES) was added to the solution, depending on the experimental condition. The solution was equally separated into two 500 ml polyethylene bottles, then either 0.684 g of $K_2HPO_4 \cdot 3H_2O$ (Alfa Aesar) or 0.834 g of $CaCl_2$ (Alfa Aesar) was added to each bottle. Both solutions were adjusted to pH 7.25 using 1 N HCl, and the volumes of the solutions were adjusted to 500 ml with deionized water.

Table S1. Ionic components of simulated body fluids and human blood plasma.

Solution	Na^+	K^+	Mg^{2+}	Ca^{2+}	Cl^-	HCO^{3-}	HPO_4^{2-}	SO_4^{2-}
1×SBF[2]	142.0	5.0	1.5	2.5	147.8	4.2	1.0	0.5
3×SBF	142.0	9.0	1.5	7.5	157.8	4.2	3.0	0.5
Human blood plasma[3]	142.0	5.0	1.5	2.5	103.0	27.0	1.0	0.5

* The pH of the 3×SBF was adjusted to 7.25 with 50 mM of Tris ($(CH_2OH)_3CNH_2$) and 1 N HCl.

For the collagen mineralization, the two solutions, separately contained in 60 mL syringes, were continuously flowed into reactor at 0.11 ml min^{-1} per syringe, using a syringe pump. To prevent any precipitation prior to the experiment, the two solutions were combined just before the reaction (Figure S1a). The volume of the solution in the reactor was 12.5 ml, giving 57 min of residence time. A hot plate maintained the reactor at 37 ± 1 ºC. Homogeneous nucleation in 3×SBF containing either 0 or 10 mg l^{-1} pAsp was not significant enough to be detectable by SAXS.

In this study, to better evaluate the different nucleation kinetics and pathways during both mineralization processes and to thoroughly investigate this complex system, we simplified the system to use one type and concentration of pAsp (10 mg l^{-1} of 5,000 Da pAsp). The addition of 10 mg l^{-1} pAsp effectively controlled mineralization patterns during the 15 h period in our experimental setup; therefore, we used this concentration throughout the study. The concentration of pAsp used here was within the ranges of previous studies evaluating the influence of pAsp on CaP mineralization: 10 mg l^{-1} was used in a study by Nudelman *et al*. for their cryogenic observations of collagen fibrils; [4] 50 mg l^{-1} was used by studies by Jee *et al*. on the biomimetic mineralization of collagen utilizing the polymer-induced liquid-precursor (PILP) process; [5,6] 1–100 mg l^{-1} was used by Cantaert *et al.*, to study the effect of pAsp on CaP precipitation in confined structures utilizing track-etch (TE) membrane pores.[7] Furthermore, we did test 100 mg l^{-1} pAsp; however, we were not able to monitor the nucleation behaviors properly due to its slow mineralization kinetics. The influences of other types of nucleation inhibitors were not tested for a similar reason. For example, fetuin, one of the most well-known NCPs, stimulates intrafibrillar mineralization, however, extrafibrillar CaP also formed simultaneously in a previous study.[4] Therefore, the use of the fetuin would not provide separate CaP nucleation pathways for intra and extrafibrillar mineralization. In addition, we expect that changes in concentration and molecular

weight of pAsp may alter the nucleation kinetics; however, we do not expect that those changes will lead to totally different nucleation pathways. Based on this study, future work can systematically evaluate the effects of molecular weights and concentrations of pAsp, or other types of nucleation inhibitors, such as non-collagenous proteins.

***In situ* X-ray scattering data collection and analysis.** Small angle X-ray scattering **(**SAXS) data were collected at the Advanced Photon Source (APS, Sector 12 ID-B) at Argonne National Laboratory (Argonne, IL, USA).[8,9] At intervals of 5, 9.5, and 15 h, frames were immediately moved to the SAXS sample stage and scanned within 5 min. By vertically moving the sample stage, each sample was scanned from $z = 0$, where the collagen matrix and simulated body fluid contact each other, to $z = 1.5$ mm depth of the matrix (Figure S1b). The distance from the sample to the SAXS detector was 3.6 m, which provided a range of 0.0017–0.53 $Å^{-1}$ for the scattering vector, q. For each scan, the sample was exposed to a 14 keV X-ray beam for 1 s. The size of the beam was 150 μm (perpendicular to the z-axis) × 40 μm (parallel to the z-axis). Two different lateral positions were scanned at each time for duplicated samples; therefore, a total of four scattering patterns were obtained for each condition and position.

The 2-dimensional scattering intensity counted by the detector (2M Pilatus) was averaged over the q range along the radial direction to produce 1-dimensional scattering intensities $I(q)$. Silver behenate powder was used as the q calibration standard. $I(q)$ was normalized by the incident beam intensities and calibrated using a reference glassy carbon standard sample, thus SAXS intensities collected from different measurements could be compared each other. The SAXS intensities were corrected by subtracting the averaged intensity of unmineralized collagen matrices (at 0 h) as a background (Figure S2).

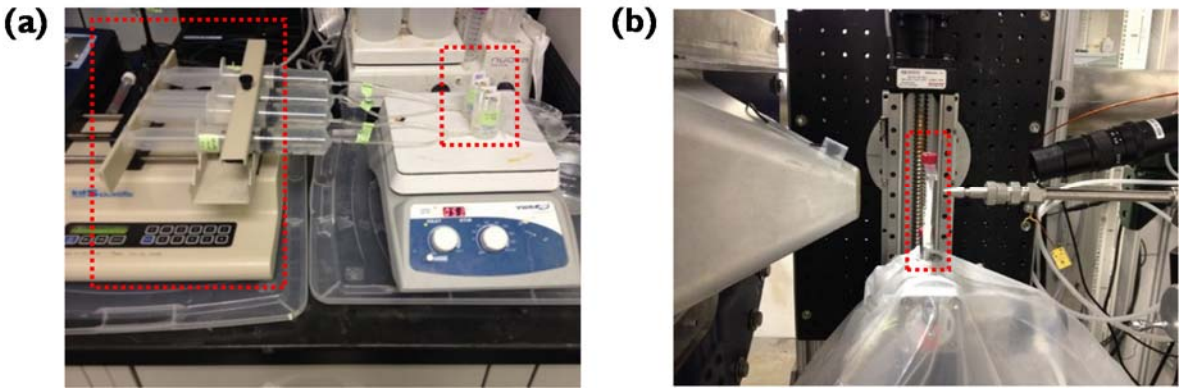

Figure S1. Experimental setup for collagen mineralization and SAXS measurements. (a) Mineralization of collagen matrices occurred within the frames in a flow-through reaction system (left dashed box: a syringe pump providing two different reaction conditions simultaneously; right dashed box: two testing frames per each condition). (b) The SAXS setup at the Advanced Photon Source sector 12-ID-B, Argonne National Laboratory (dashed dox: testing frame, viewed from the side, as in Figure 1b).

Total particle volume was estimated from the linear relationship with invariant values, Q, as shown in eq. S1. Integration was conducted within a limited q range of 0.0017–0.2 $Å^{-1}$, due to the relatively high noise in larger q regions.

$$Q = \left(\frac{1}{2\pi^2}\right) \int q^2 I(q) dq \qquad \text{eq. S1}$$

The Modelling II tool of the IRENA package written in IGOR Pro (WaveMetrics Inc.) was provided by APS and used for the data analysis to fit the SAXS pattern. The equations used in the fitting are summarized below, and more detailed information can be found elsewhere.[10] Absolute volume fractions of CaP particles in collagen matrices were obtained by the fitting of $I(q)$ calibrated on an absolute scale using a reference glassy carbon standard sample.[11] The structural factor was assumed to be 1. Using a two-population model of this Modelling II in the IRENA

package, $I(q)$ can be evaluated as a sum of spherical and platy calcium phosphate (CaP) populations. In the absence of collagen fibrils, the spherical CaP was reported to appear as a precursor to crystalline apatite at the initial stage of nucleation.[12,13] A unified level tool was for the evaluation of spherical populations with fractal dimensions and a fitting tool using form factor was used for considering platy shape particle population in the Modelling II. First, spherical populations with fractal dimensions can represent the aggregation behavior during particle formation. In this model, $I(q)$ can be expressed as eq. S2.[10,14]

$$I(q) = G \exp\left(-\frac{q^2 R_g^2}{3}\right) + B(q^*)^{-P}. \qquad \text{eq. S2}$$

where, $q^* = \frac{q}{[\mathrm{erf}(\frac{q\,R_g}{\sqrt{6}})]^3}$, R_g is the radius of gyration, and B is the constant prefactor specific to the type of power-law scattering. A power-law scattering exponent P can be evaluated from the slope of log(I) vs. log(q) at high q. For typical monodisperse spheres following Porod's law, $P = 4$. For $P = 1$–3, particles are considered to have mass fractal structures with fractal dimensions, D_f, equal to P. Spherical aggregates typically show $D_f \sim 3$.[14,15] The exponential prefactor, G, can provide volume fractions of the particles from the eq. S3.

$$G = n\, r_e^2 \Delta\rho^2 V^2, \qquad \text{eq. S3}$$

where n is the number concentration of particles and V is the volume of a particle ($V = (\frac{2{,}000\,\pi^2}{243} R_g^6)^{\frac{1}{2}}$). r_e and Δρ represent the classical electron radius (2.818 fm) and the difference in electron densities between particles and the medium, respectively. Therefore, from the fitting parameters of G, and R_g, the particle volume fractions of a spherical CaP population, V_{sp}, can be evaluated by n multiplied by V.

For fitting the plate CaP population with thickness, *t*, another fitting tool using a built-in form factor (a unified disk, eq. S4[16]) and a size distribution function in the Modelling II package was used.

$$|F(q,R)|^2 = A + G1\ exp^{-\frac{q^2 {R_g 1}^2}{3}} + \frac{B1}{q*^4} \qquad \text{eq. S4}$$

where R is the radius of the plate, $\mathrm{A} = exp^{-\frac{q^2 {R_g 2}^2}{3}} + \frac{2}{R^2 {Q_{SV}}^2}\ e^{-\frac{(1.1 R_g 1)^2 q^2}{3}}$, $q* = \frac{q}{[\mathrm{erf}(\frac{q R_g 1}{\sqrt{6}})]^3}$, $\mathrm{B1} = 4\frac{t+R}{R^3 t^2}$, $\mathrm{G1} = 2\frac{t^2}{3R^2}$, $R_g 1 = \frac{\sqrt{3}\,t}{2}$, and $R_g 2 = \sqrt{(\frac{R^2}{2} + \frac{t^2}{12})}$. Then, SAXS intensity was calculated by a summation over a discrete size histogram with eq. S5:

$$I(q) = r_e^2 |\Delta\rho|^2 \sum_i |F(q,R_i)|^2 V(R_i) f(R_i) \Delta R_i \qquad \text{eq. S5}$$

In eq. S5, the subscript *i* includes all bins in the size distribution, and ΔR_i is the width of bin *i*. $V(R)$ is the particle volume, and $f(R)$ is the volume size distribution, which can be related to the number size distribution by

$$f(R) = V(R) n P(R), \qquad \text{eq. S6}$$

where $P(R)$ is the probability of occurrence of a scatter of radius R. For the lognormal distribution,

$$P(R) = \frac{1}{\sigma R\sqrt{2\pi}} e^{-\frac{(\ln(R-\mu))^2}{2\sigma^2}}, \qquad \text{eq. S7}$$

where μ is the mean radius in number size distribution, and σ is the standard deviation. For the fitting, μ, σ, and n were first fitted, and then the particle volume fractions of platy CaP population, V_{pl} was obtained by $\sum_i V(R_i) n P(R) \Delta R_i$.

The scattering contrast, Δρ, was estimated from difference between the electron densities, ρ, of CaP and water, ($\rho_{\mathrm{CaP}} - \rho_{\mathrm{water}}$). $\rho = \sum C_z f_z$ for all elements, where, C_z is the atomic

concentration and f_z is the scattering factor, which is equivalent to the atomic number for SAXS analysis. For the spherical population, CaP was assumed to be amorphous ($Ca_9(PO_4)_6$, known as a Posner's cluster, with a specific gravity of 1.75[17, 18], yielding $\Delta\rho = 1.89 \times 10^{23}$ cm^{-3}. A recent study by Habraken *et al*.[12] estimates the structure of post-nucleation clusters as $[Ca_2(HPO_4)_3]^{2-}$, which provides an almost similar $\Delta\rho$ (1.93×10^{23} cm^{-3}). For the CaP platy population, the structure of CaP is assumed to be a hydroxyapatite crystal ($Ca_5(PO_4)_3OH$ with a specific gravity of 3.16), yielding $\Delta\rho = 6.12 \times 10^{23}$ cm^{-3}. Although hydroxyapatite is known to most closely approximate bone crystals, octacalcium phosphate (OCP) is frequently proposed as the early stage of platy CaP for bone.[12] The assumption that platy particles are OCP ($Ca_8H_2(PO_4)_6 \cdot 5H_2O$, with a specific gravity of 3.16) also provides little change in $\Delta\rho$ (6.22×10^{23} cm^{-3}). Therefore, the errors resulting from assumptions of the structure of spherical and platy particles are expected to be about 4%.

Similarly, *in situ* wide angle X-ray scattering (WAXS) data was collected at APS sector 11-ID-B to identify the CaP phases during collagen mineralization. Collagen matrices were exposed to a 58.66 keV X-ray beam for 5 min (2 s × 150 times) during flow-through mineralization reaction. The beam size was 300 μm in both the lateral and vertical dimensions. The 2-dimensional WAXS intensities were counted by a Perkin Elmer amorphous silicon detector, which was 20 cm away from the sample, providing information at q higher than 0.6 Å^{-1}. Then the 2-dimensional intensities were averaged over the q range along the radial direction to produce 1-dimensional scattering intensities $I(q)$, using FIT2D software provided by the European Synchrotron Radiation Facility. Cerium dioxide was used as the calibration standard.

***Ex situ* analyses of collagen mineralization.** Thin sections (100 nm) of the matrices were prepared for TEM analysis. Matrices were fixed in 100 mM cacodylate buffer containing 2% paraformaldehyde and 2.5% glutaraldehyde. The matrices were rinsed in a cacodylate buffer

solution and then fixed with 1% osmium tetroxide in the buffer solution for 1 h. After dehydration in successive ethanol baths (30, 50, 70, 90, and 95 % for 15 min each, and 100% for 15 min × 3 times), samples were embedded in epoxy resin and thin sections were prepared using an ultramicrotome (EM UC7, Leica). Uranyl acetate and Reynold's lead citrate were used for staining before the analysis. For TEM imaging without staining, treatments using osmium tetroxide, uranyl acetate, and lead citrate were omitted during the sample preparation. Two different instruments were used for TEM imaging. A JEOL 1200 EX II was operated at 100 kV, and a JEOL JEM-2100F was operated at 200 kV for higher resolution images.

Collagen matrices and films were placed in an ethanol bath for 5 h to remove excess ions, then stored at 4 ^{o}C until *ex situ* analyses by Raman spectroscopy and scanning electron microscopy (SEM) equipped with energy-dispersive X-ray spectroscopy (EDS). Additionally, matrices were frozen in liquid nitrogen and cut into ~1 mm thick sections for the analysis along the *z*-direction (Figure S6a). These sections were air-dried on either glass slides, for Raman spectroscopy, or on SEM specimen stubs covered with carbon tape, for SEM imaging. Using a 50× objective lens, Raman spectra were collected (inVia Raman spectrometer, Renishaw plc) at each position, with corresponding optical images. A spectral range from 100 to 3,700 Δcm^{-1} was used, and simultaneously detected with a spectral resolution of 1.13 Δcm^{-1}, using 514 nm laser excitation focused on the sample surface. Samples dried on the SEM stubs were sputter-coated with Au-Pd under Ar at 0.2 mbar (Cressington 108) to increase conductivity, then imaged with a 10 kV electron accelerating voltage at a 5−6 mm working distance (FEI Nova NanoSEM 2300).

Fluorescence correlation spectroscopy (FCS) was used to evaluate the pore structures of the matrices by measuring the diffusion time of rhodamine 6G (R6G). R6G was chosen for its small size (MW = 479.02 g mol^{-1}), photostability, and high fluorescence quantum yield. FCS

measurement was performed using an inverted design confocal laser scanning microscope (Zeiss Axiovert 200M) equipped with a 40× water immersion lens. R6G molecules were excited by a 514 nm argon laser. Fluorescence intensities were collected for 30 s × 10 times, then the diffusion time was evaluated by analyzing correlation curves. Two different locations were evaluated from each *z*-position in each sample. The time shift τ was varied, and the correlation curve was obtained by multiplying the deviation of the average intensity, *I*, at the time point *t*, by the deviation at time point $t + \tau$, and then averaging over the whole trace. Finally, the correlation function, $G(t)$, was normalized to the squared average signal.[19,20]

$$G(\tau) = \frac{<I(t)I(t+\tau)>}{<I(t)>^2} - 1 \qquad \text{eq. S8}$$

The diffusion time, τ_D, and number of fluorescent molecules in the detection volume, *N*, of a given component, *i*, are commonly fitted with the standard model:

$$G(\tau) = \frac{1}{N}\sum_i \varphi_i \left(1 + \frac{\tau}{\tau_{D,i}}\right)^{-1}\left[1 + \left(\frac{\omega_0}{z_0}\right)^2 \frac{\tau}{\tau_{D,i}}\right]^{-\frac{1}{2}}, \qquad \text{eq. S9}$$

where φ_i characterizes the fraction of molecules of the component, and ω_0, and z_0 are Gaussian profiles of the detected volumes in the x-y directions. τ_D can be correlated with the diffusion coefficient, D, using the following equation:

$$\tau_D = \frac{\omega_0^2}{4D}. \qquad \text{eq. S10}$$

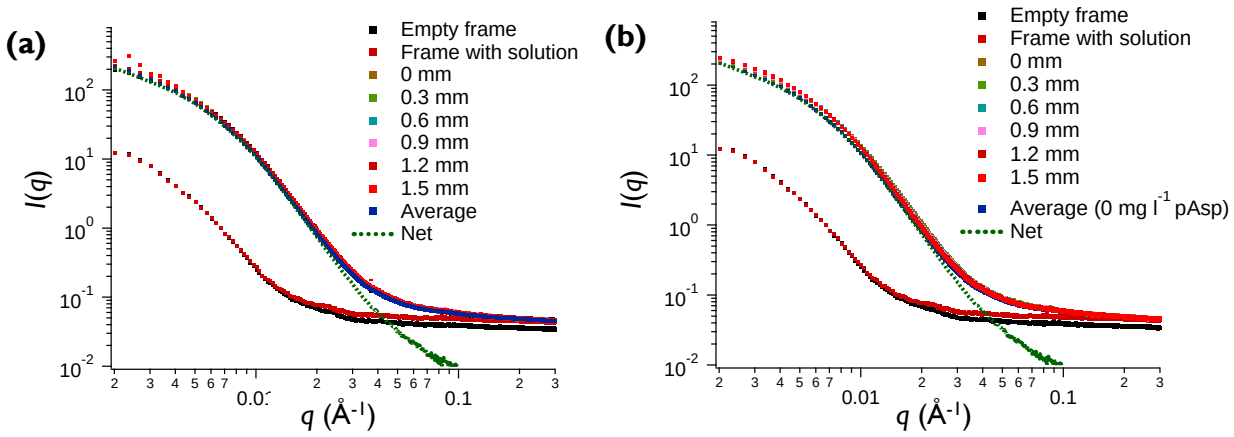

Figure S2. Background SAXS intensities. (**a**) SAXS intensities were measured for an empty frame with cover glass, a frame filled with 3×SBF solution with no Ca^{2+} ions, and a frame with an unmineralized collagen matrix at z = 0–1.5 mm. Before the analysis, unmineralized collagen matrices were stored overnight in 3×SBF solutions with no Ca^{2+} ions. There was little difference in SAXS intensities for unmineralized collagen at different z-positions. The net intensity (green dotted line) indicates the scattering from collagen, and was obtained by subtracting scattering of solution and frames (Frame with solution) from unmineralized collagen matrix (Average). (**b**) The addition of 10 mg l^{-1} pAsp in SBF did not affect the intensities of the unmineralized matrix. The averaged values of intensities from unmineralized collagen at z = 0–1.5 mm (**a**) were used as the background intensity for all analyses of SAXS intensities in the subsequent experiments.

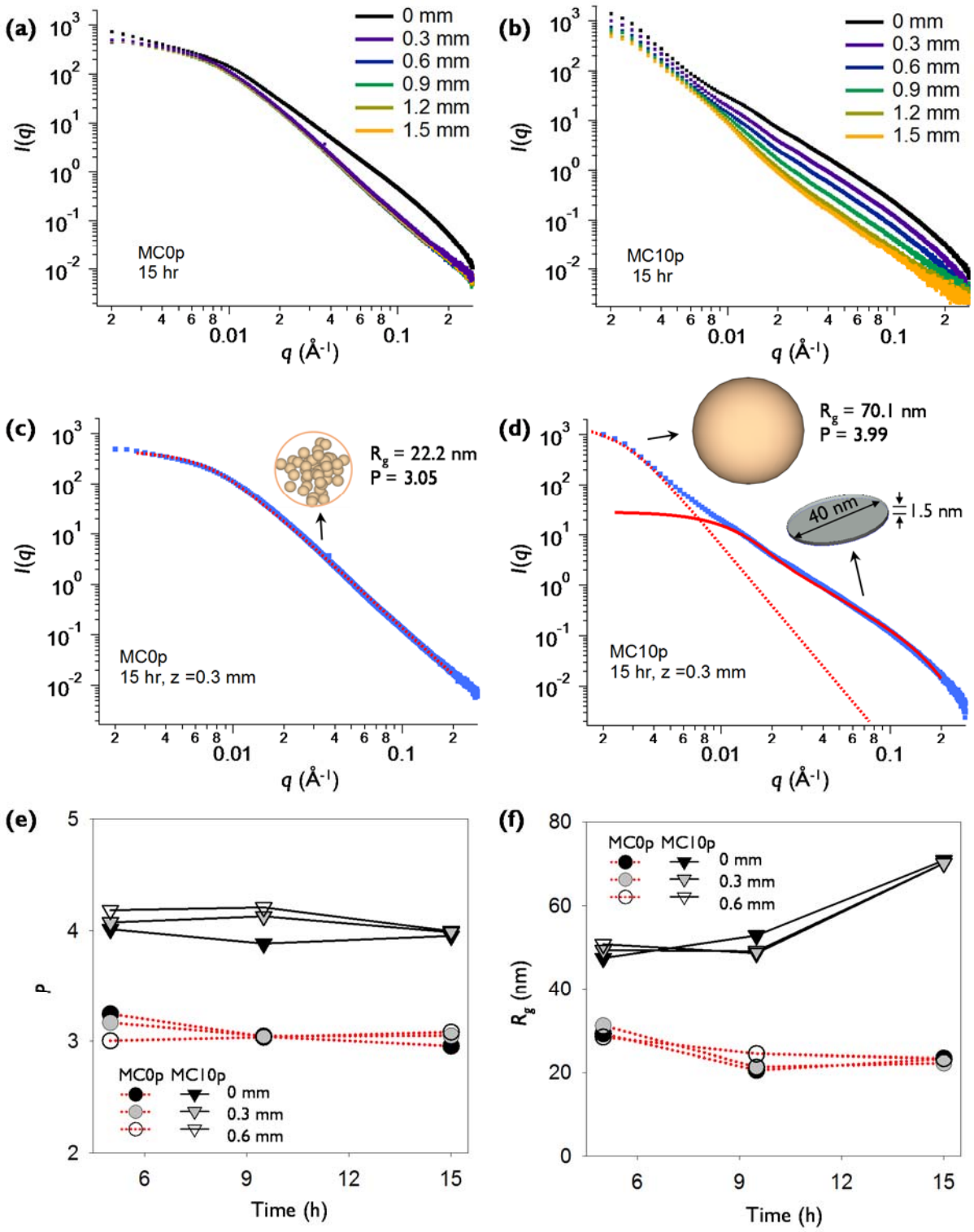

Figure S3. SAXS intensities from mineralized collagen matrices and their fittings. SAXS intensities from MC0p (**a**) and MC10p (**b**) at z = 0–1.5 mm at 15 h of mineralization. (**c**, **d**) Examples of fittings for SAXS intensities at z = 0.3 mm at 15 h (thick blue lines) using a model of

two populations of plates and spheres. (**c**) The fitting of SAXS pattern from MC0p (the red dotted line overlaps with the raw intensity indicated by the blue line) indicated that CaP particles were aggregated spheres (the power-law scattering exponent, P = 3.05) with R_g = 22.2 nm. The contribution of the platy CaP population was minimal. (**d**) The fitting of the SAXS pattern from MC10p shows that populations of plates and spheres co-exist. The SAXS intensity at large q fits 1.5 nm thick plates with a diameter of 40 nm (standard deviation of 0.15 in log-normal distribution). The obtained morphology of plates closely approximates known bone crystalline dimensions.[21,22] These morphologies were used for fitting the total particle volume fractions of the plate population from other SAXS patterns at different depths and time. Another population of spheres of R_g = 70.1 nm appears at small q, with a P fitting to 3.99, which indicates that particles were typical surface scatter, not formed from aggregation of primary particles or nucleation precursors. (**e**, **f**) P and R_g values for the spherical population fitted from SAXS intensities from MC0p and MC10p at z = 0–0.6 mm over time.

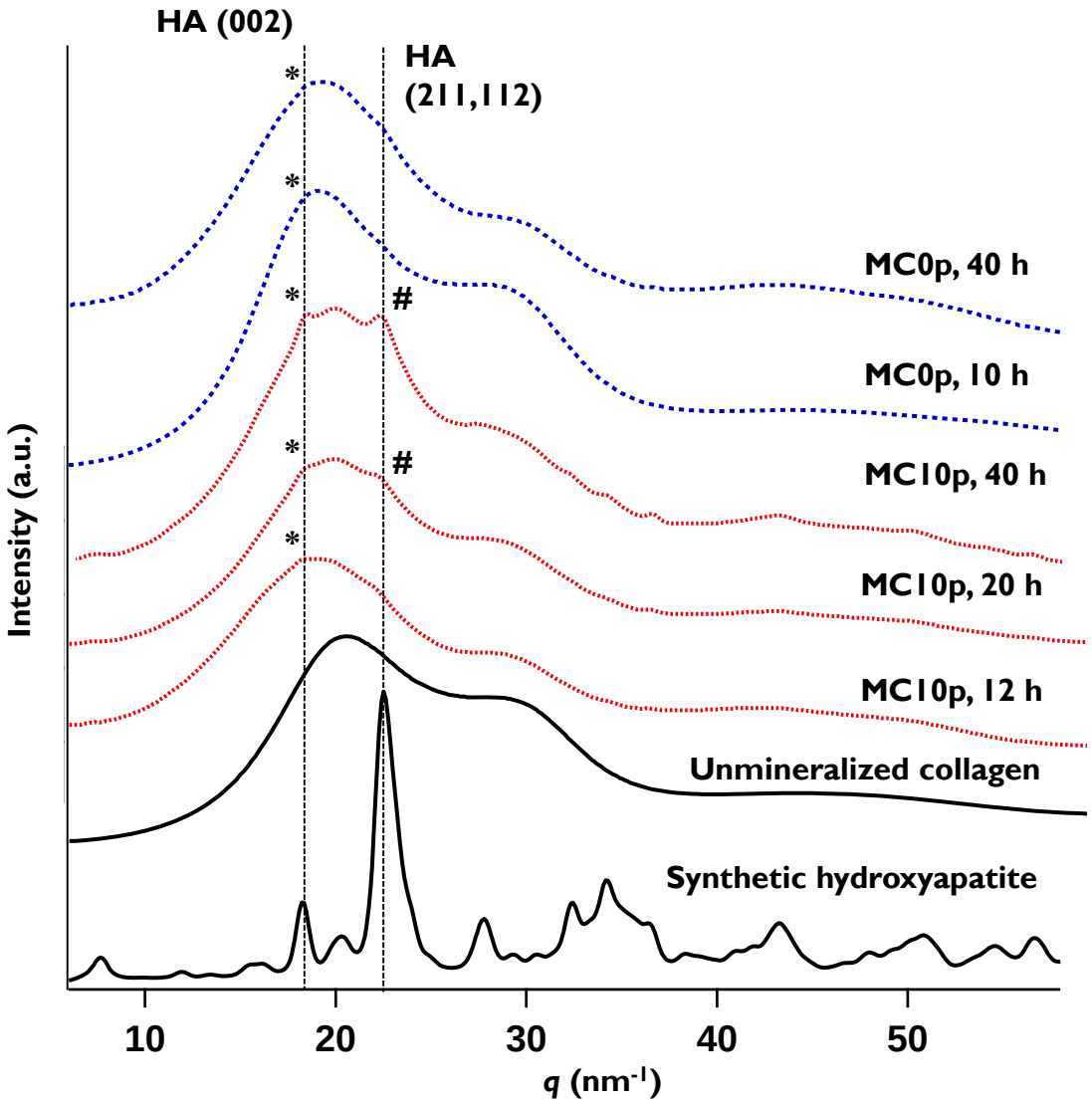

Figure S4. WAXS patterns from mineralized collagen matrices at *z* = 0–0.3 mm and from synthetic hydroxyapatite (HA). Until 10–12 h, a peak of WAXS intensity appeared only at q ~ 18.25 nm^{-1}, which corresponds to the (002) face of HA (d-spacing: 3.442 Å, indicated as *) from both MC0p and MC10p. After 20 h, more peaks matching with HA appeared distinctively only from MC10p, including one at q ~ 22.5 nm^{-1} for the (211) and (112) faces of HA (d-spacing: 2.813 and 2.778 Å, respectively, indicated as #).

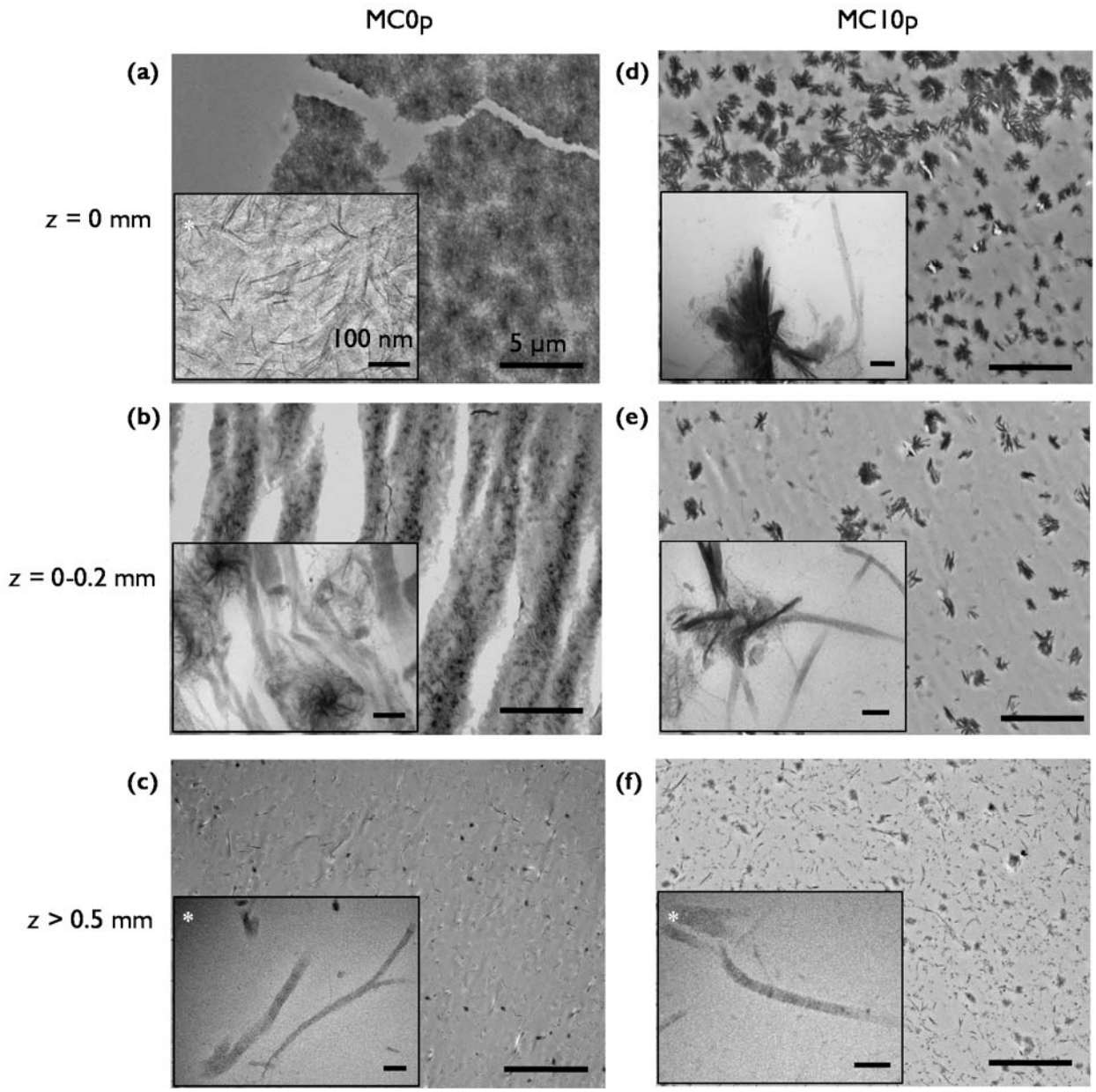

Figure S5. **TEM images of stained thin sections of MC0p (a-c) and MC10p (d-f) at a late stage of mineralization.** Samples were prepared after 15 h of mineralization for *in situ* SAXS analysis, followed by an additional 23 h incubation in 3×SBF to evaluate how changes in diffusion of nucleation and growth precursors influence CaP distribution in the extrafibrillar space at the later stage (See also Figure 7). Insets are high resolution images corresponding to features in **a**-**f**. Scale bars in **a**-**f** are 5 µm, and those in insets are 100 nm. The * symbols indicate that images were taken at an acceleration voltage of 200 kV. Other images were taken at 100 kV. The

indicated *z*-positions are approximate because collagen matrices lost their original forms owing to dehydration during the thin section preparation. Near the area of the solution–collagen matrix interface, for MC10p samples, banding patterns are nearly absent from collagen fibrils due to intrafibrillar mineralization (the inset in **d**). Banding is still visible in MC0p samples (the inset in **b**). In the interior of the matrices (z > 0.5 mm), where few extrafibrillar particles present, collagen fibrils appear similar in both groups, with ambiguity between CaP particles and precipitations of staining molecules (the insets in **c** and **f**).

Ex situ analyses of CaP distribution within the collagen matrices at a late stage of mineralization

To better evaluate the CaP distribution within the collagen matrices at a late stage of mineralization, sections cut along the *z*-direction of MC0p and MC10p (Figure S6a) were analyzed using SEM-EDS and Raman spectroscopy. The surface of the MC0p section was mostly covered with a layer of CaP minerals, and collagen matrix was located below and slightly visible through narrow gaps in the mineral layer (Figure S6b). Possibly, the collagen fibrils had shrunk to the bottom during dehydration for sample preparation, while relatively mobile extrafibrillar CaP particles were more densely aggregated on top. The EDS analyses of MC0p sections (Table S2) showed distinctly different characteristics for the mineral layer (Figure S6d,g) and the surface of the collagen matrix without visible particles (Figure S6f). Ca/P ratios from the mineral layer were 1.2–1.38, which are close to that of OCP (1.33). This range is expected to appear during the early stage apatite (Ca/P = 1.67) development process.[12] However, Ca and P were not detected on the surface of the collagen matrix at $z = 0.3$ mm, where no extrafibrillar particles were visible (Figure S6f). This demonstrates that intrafibrillar mineralization was not achieved, even after the additional 23 h of reaction after the initial 15 h experiment.

Unlike the MC0p samples, the surfaces of the MC10p were clearly exposed, rather than entirely covered by a mineral layer (Figure S6c), due to the inhibition of extrafibrillar CaP formation by pAsp. The MC10p surfaces without extrafibrillar CaP particles (indicated as 'IM' in Figures S6e,h) clearly showed Ca and P signals, proving that the addition of pAsp promoted intrafibrillar mineralization. There would be little chance that extrafibrillar CaP particles were hidden below the collagen fibrils and detected by the surface sensitive SEM-EDS because most collagen fibrils located below the extrafibrillar CaP layers as shown in Figure 6b. Even with more extrafibrillar CaP particles during the mineralization without pAsp, no Ca and P signal was detected from exposed collagen surfaces (Figure 6f). The Ca/P ratios from mineralized collagen matrices (Ca/P = 0.84–1.0) were lower than that of OCP, but similar to that of the amorphous phase (typically less than 1[12]). However, we did not conclude that CaP crystals embedded inside the collagen fibrils are amorphous. SEM-EDS has a low resolution compared to the size of nanoscale intrafibrillar CaP plates, raising the possibility that Ca and P signals were detected from other parts of the collagen matrices. In sum, we found that the Ca/P ratios of the extrafibrillar

particles were close to those of OCP or apatite. In the presence of pAsp, the Ca/P ratio in collagen matrices reflected mineralization, while in the absence of pAsp, neither Ca nor P was detected from the collagen surface without extrafibrillar particles (Figure S6f). Thus, it is evident that IM was promoted only with the addition of pAsp.

Raman spectra analyzed from multiple spots throughout the MC10p surface at z = 0.3 mm (Figure S6h) showed a regular pattern characteristic of phosphate peaks at Δ960 cm^{-1} (the P–O band for apatite in the solid box in Figures S6i, j) and collagen peaks at Δ2,941cm^{-1} (the C–H band for collagen in the dotted box in Figure S6i). These spectral patterns are consistent with mineralized tendons or bone samples.[23,24] However, Raman spectra from the exposed collagen area from the MC0p sample (Figure S6f) did not have peaks at Δ960 cm^{-1} (Figures S6i,j), indicating no apatite was formed within the collagen fibrils without extrafibrillar particles. Instead, these areas showed distinct collagen signatures, with higher intensities at Δ2,941cm^{-1} and clear minor peaks at Δ1,451cm^{-1} (the C–H band for collagen) and at Δ1,667cm^{-1} (the C=O band for collagen). The Raman spectra analyses also confirmed that IM was facilitated only with the presence of pAsp.

Ex situ evaluations using Raman spectra (by providing the development of P–O banding) and SEM-EDS (by providing Ca/P ratio; estimation of elemental composition in macroscale) in this study can help to identify the CaP phases. However, the direct comparison of the above information with *in situ* WAXS analysis should take a careful approach because the WAXS analysis can provide additional information about the development of each lattice structure of specific mineral (i.e., both short- and long- range order information). As shown in Figure S4, only amorphous status of extrafibrillar CaP was observed from MC0p, thus, we conclude that extrafibrillar CaP aggregates, developed during the *in situ* mineralization without pAsp, are mostly amorphous, but they can transform into apatite minerals when further mineralized.

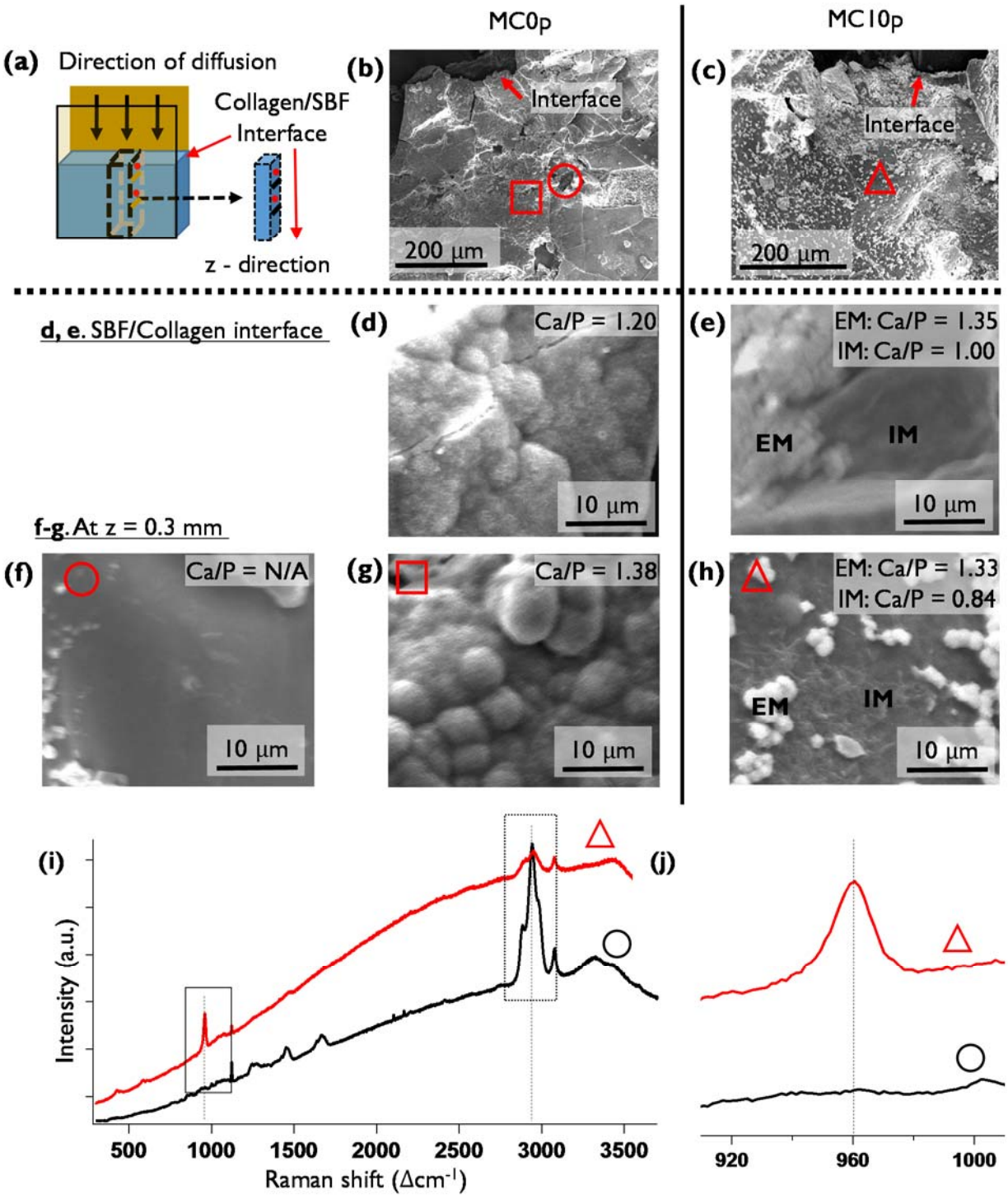

Figure S6. SEM images and corresponding Raman spectra of collagen matrices. Samples were analyzed after 15 h of mineralization for *in situ* SAXS analysis, followed by an additional 23 h incubation in 3×SBF. (**a**) Schematic illustration of sample preparation for evaluating the cross

section of the matrices. Samples were frozen in liquid nitrogen before cutting sections. SEM low resolution images of a section of (**b**) MC0p and (**c**) MC10p. (**d**-**h**) High resolution SEM images of selected areas indicated in **b** and **c**. Ca/P ratios were evaluated by SEM-EDS. (**d**) A layer of aggregated CaP plates on MC0p at z = 0 mm. (**e**) Mineralized collagen of MC10p at *z* = 0 mm with scattered extrafibrillar CaP. (**f**) Unmineralized collagen matrix of MC0p at *z* = 0.3 mm (circle in **b**). (**g**) A layer of aggregated CaP plates on MC0p at z = 0.3 mm (square in **b**). (**h**) Mineralized collagen of MC10p at *z* = 0.3 mm, with a few scattered extrafibrillar CaP (triangle in **c**). **EM** and **IM** indicate the extrafibrillar CaP and the surface of mineralized collagen matrix, respectively. (**i**) Raman spectra of selected positions indicated in **b** and **c**. The black and red lines correspond to **f** (circle in **b**) and **h** (triangle in **c**), respectively. (**j**) Enlarged area of Raman spectra (left box in **i**) showing phosphate-specific peaks at Δ960 cm^{-1}.

Table S2. Atomic ratios of mineralized collagen at different positions on cross sections, from SEM-EDS.

Sample	MC0p			MC10p			
z (mm), Fig. S6*	0, **d**	0.3, **f**	0.3, **g**	0, **e**-EM	0, **e**-IM	0.3, **h**-EM	0.3, **h**-IM
C	35.5	69.1	34.3	42.0	64.2	42.4	62.8
N	-	13.3	-	7.4	16.0	9.4	12.9
O	29.4	15.5	36	30.6	16.1	31.6	18.5
Na	10.1	0.7	5.8	2.0	0.6	1.7	1.0
Cl	9.6	1.4	5.7	2.0	1.3	1.6	1.3
Ca	**8.4**	**-**	**10.5**	**9.2**	**1.0**	**7.6**	**1.6**
P	**7.0**	**-**	**7.6**	**6.8**	**1.0**	**5.7**	**1.9**
Ca/P**	**1.20**	**N/A**	**1.38**	**1.35**	**1.0**	**1.33**	**0.84**

* Figure labels in Fig. S6

** Ca/P for OCP and apatite are 1.33 and 1.67, respectively.

References

(1) Boyle, J. J.; Kume, M.; Wyczalkowski, M. A.; Taber, L. A.; Pless, R. B.; Xia, Y.; Genin, G. M.; Thomopoulos, S. J. *J. R. Soc. Interface* 2014, 11.

(2) Ohtsuki, C.; Kokubo, T.; Yamamuro, T. *J. Non-Cryst. Solids* 1992, 143, 84-92.

(3) Gamble, J. L. *Chemical Anatomy Physiology and Pathology of Extracellular Fluid*: 6th ed.; Harvard University Press: Cambridge, MA, 1967.

(4) Nudelman, F.; Pieterse, K.; George, A.; Bomans, P. H. H.; Friedrich, H.; Brylka, L. J.; Hilbers, P. A. J.; de With, G.; Sommerdijk, N. A. J. M. *Nat. Mater.* 2010, 9, 1004-1009.

(5) Jee, S.-S.; Thula, T. T.; Gower, L. B. *Acta Biomater.* 2010, 6, 3676.

(6) Jee, S. S.; Culver, L.; Li, Y.; Douglas, E. P.; Gower, L. B. *J. Cryst. Growth* 2010, 312, 1249-1256.

(7) Cantaert, B.; Beniash, E.; Meldrum, F. C. *J. Mater. Chem.B* 2013, 1, 6586.

(8) Jun, Y.-S.; Lee, B.; Waychunas, G. A., *Environ. Sci. Technol.* 2010, 44, 8182-8189.

(9) Li, Q.; Fernandez-Martinez, A.; Lee, B.; Waychunas, G. A.; Jun, Y.-S., *Environ. Sci. Technol.* 2014, 48, 5745-5753.

(10) Ilavsky, J.; Jemian, P. R. *J. Appl. Crystallogr.* 2009, 42, 347-353.

(11) Zhang, F.; Ilavsky, J.; Long, G.; Quintana, J. G.; Allen, A.; Jemian, P. *Metall. Mat. Trans. A* 2010, 41, 1151-1158.

(12) Habraken, W. J. E. M.; Tao, J.; Brylka, L. J.; Friedrich, H.; Bertinetti, L.; Schenk, A. S.; Verch, A.; Dmitrovic, V.; Bomans, P. H. H.; Frederik, P. M.; Laven, J.; van der Schoot, P.; Aichmayer, B.; de With, G.; DeYoreo, J. J.; Sommerdijk, N. A. J. M. *Nat. Commun.* 2013, 4.

(13) Dey, A.; Bomans, P. H.; Müller, F. A.; Will, J.; Frederik, P. M.; Sommerdijk, N. A. *Nat. Mater.* 2010, 9, 1010-1014.

(14) Beaucage, G.; Kammler, H. K.; Pratsinis, S. E. *J. Appl. Crystallogr.* 2004, 37, 523-535.

(15) Fratzl, P. *J. Appl. Crystallogr.* 2003, 36, 397-404.

(16) Beaucage, G. *J. Appl. Crystallogr.* 1995, 28, 717-728.

(17) Betts, F.; Posner, A. S. *Mater. Res. Bull.* 1974, 9, 353-360.

(18) Combes, C.; Rey, C. *Acta Biomater.* 2010, 6, 3362-3378.

(19) Kihara, T.; Ito, J.; Miyake, J. *PLoS ONE* 2013, 8, e82382.

(20) Rigler, R.; Mets, Ü.; Widengren, J.; Kask, P. *Eur. Biophys. J.* 1993, 22, 169-175.

(21) Liu, Y.; Thomopoulos, S.; Chen, C.; Birman, V.; Buehler, M. J.; Genin, G. M. *J. R. Soc. Interface* 2014, 11.

(22) Landis, W. J.; Song, M. J.; Leith, A.; McEwen, L.; McEwen, B. F. *J. Struct. Biol.* 1993, 110, 39-54.

(23) Schwartz, A. G.; Pasteris, J. D.; Genin, G. M.; Daulton, T. L.; Thomopoulos, S. *PLoS ONE* 2012, 7, e48630.

(24) Wopenka, B.; Kent, A.; Pasteris, J. D.; Yoon, Y.; Thomopoulos, S. *Appl. Spectrosc.* 2008, 62, 1285-1294.